Separation and single-cell analysis for free gastric cancer cells in ascites and peritoneal lavages based on microfluidic chips

Junhua Zhao,[b,c,d,e] Zhaojun Han,[a,e] Chang Xu,[a,e] Lu Li,[a,****] Haimeng Pei,[a] Yongxi Song,[b,c,d,***] Zhenning Wang,[b,c,d,**] and Bo Tang[a,*]

[a]College of Chemistry, Chemical Engineering and Materials Science, Key Laboratory of Molecular and Nano Probes, Ministry of Education, Collaborative Innovation Center of Functionalized Probes for Chemical Imaging in Universities of Shandong, Institute of Molecular and Nano Science, Shandong Normal University, Jinan, 250014, PR China
[b]Department of Surgical Oncology and General Surgery, The First Hospital of China Medical University, 155 N. Nanjing Street, Shenyang, Liaoning, 110001, PR China
[c]Key Laboratory of Precision Diagnosis and Treatment of Gastrointestinal Tumors, Ministry of Education, China Medical University, No.77, Puhe Road, Shenyang, Liaoning, 110001, PR China
[d]Institute of Health Sciences, China Medical University, No.77, Puhe Road, Shenyang, Liaoning, 110001, PR China

eBioMedicine
2023;90: 104522
Published Online xxx
https://doi.org/10.1016/j.ebiom.2023.104522

Summary

Backgrounds Detecting free cancer cells from ascites and peritoneal lavages is crucial for diagnosing gastric cancer (GC). However, traditional methods are limited for early-stage diagnosis due to their low sensitivity.

Methods A label-free, rapid, and high-throughput technique was developed for separating cancer cells from ascites and peritoneal lavages using an integrated microfluidic device, taking advantage of dean flow fractionation and deterministic lateral displacement. Afterward, separated cells were analyzed using a microfluidic single-cell trapping array chip (SCTA-chip). In situ immunofluorescence for EpCAM, YAP-1, HER-2, CD45 molecular expressions, and Wright-Giemsa staining were performed for cells in SCTA-chips. At last, YAP1 and HER-2 expression in tissues was analyzed by immunohistochemistry.

Findings Through integrated microfluidic device, cancer cells were successfully separated from simulated peritoneal lavages containing 1/10,000 cancer cells with recovery rate of 84.8% and purity of 72.4%. Afterward, cancer cells were isolated from 12 patients' ascites samples. Cytological examinations showed cancer cells were efficiently enriched with background cells excluded. Afterwards, separated cells from ascites were analyzed by SCTA-chips, and recognized as cancer cells through $EpCAM^{+}/CD45^{-}$ expression and Wright-Giemsa staining. Interestingly, 8 out of 12 ascites samples showed $HER\text{-}2^{+}$ cancer cells. At last, the results through a serial expression analysis showed that YAP1 and HER-2 have discordant expression during metastasis.

Interpretation Microfluidic Chips developed in our study could not only rapidly detect label-free free GC cells in ascites and peritoneal lavages with high-throughput, they could also analyze ascites cancer cells at the single-cell level, improving peritoneal metastasis diagnosis and investigation of therapeutic targets.

Funding This research was supported by National Natural Science Foundation of China (22134004, U1908207, 91859111); Natural Science Foundation of Shandong Province of China (ZR2019JQ06); Taishan Scholars Program of Shandong Province tsqn (201909077); Local Science and Technology Development Fund Guided by the Central Government (YDZX20203700002568); Applied Basic Research Program of Liaoning Province (2022020284-JH2/1013).

Keywords: Gastric cancer; Peritoneal metastasis; Microfluidic chips; Cell separation; Single-cell analysis

*Corresponding author. College of Chemistry, Chemical Engineering and Materials Science, Collaborative Innovation Center of Functionalized Probes for Chemical Imaging, Key Laboratory of Molecular and Nano Probes, Ministry of Education Shandong Normal University, Jinan 250014, P. R. China.
**Corresponding author. Department of Surgical Oncology and General Surgery, The First Hospital of China Medical University, 155 N. Nanjing Street, Shenyang, Liaoning, 110001, PR China.
***Corresponding author. Department of Surgical Oncology and General Surgery, The First Hospital of China Medical University, 155 N. Nanjing Street, Shenyang, Liaoning, 110001, PR China.
****Corresponding author. College of Chemistry, Chemical Engineering and Materials Science, Collaborative Innovation Center of Functionalized Probes for Chemical Imaging, Key Laboratory of Molecular and Nano Probes, Ministry of Education Shandong Normal University, Jinan 250014, P. R. China.
E-mail addresses: tangb@sdnu.edu.cn (B. Tang), znwang@cmu.edu.cn (Z. Wang), yxsong@cmu.edu.cn (Y. Song), lilu5252@163.com (L. Li).
[e]These authors contributed equally to this work.

Research in context

Evidence before this study

As one of the most common cancers, gastric cancer is a big medical challenge worldwide. The difficulty in diagnosing peritoneal metastasis at early stage contributed a lot to the poor prognosis of gastric cancer. Separation and identification of free cancer cells from the abdominal cavity plays a vital role in diagnosing peritoneal metastasis. In traditional clinical practice, cytological examinations were performed on ascites and peritoneal lavages to detect free cancer cells. However, this conventional method lacks sensitivity due to the difficulty for pathologists to distinguish the small number of GC cells from the background cells. In addition, GC cells have a similar tissue origin as some background cells such as mesothelial cells, limiting the usefulness of cell sorting methods such as CellSearch which rely on epithelial cell markers. Moreover, although targeted therapy is applied to control metastasis, molecular status is usually evaluated in the primary lesions since metastatic lesions are difficult to biopsy, especially for peritoneal metastasis. Thus, to improve early diagnosis and advance therapeutic strategies for GC peritoneal metastasis, new methods are needed to separate cancer cells from ascites and peritoneal lavages rapidly and label-freely as well as to investigate the molecular status of the separated cancer cells at the single-cell level.

Added value of this study

In our study, we report a label-free, rapid, and high-throughput method to diagnose peritoneal metastasis by cancer cell separation from ascites and peritoneal lavages based on an integrated microfluidic device combining dean flow fractionation and deterministic lateral displacement techniques. Our methods could concentrate cancer cells with high throughput, making it easier for pathologists to find cancer cells and improve the low sensitivity that is an always-present drawback of traditional detection methods. The separated cancer cells were also able to be identified and analyzed at the single-cell level using a microfluidic single-cell trapping array (SCTA)-chip. The separated cells were identified as cancer cells based on their CD45-negative, EpCAM-positive expression through in situ immunofluorescence. Moreover, our study detected HER-2 and YAP1 expression in ascites cancer cells at the single cell level. Interestingly, 8 out of 12 ascites samples showed HER-2^{+} in cancer cells, well higher than the HER-2 positivity detected in primary GC tissues by previous studies. We also performed a serial YAP1 and HER-2 expression analysis in four different kinds of tissues or cells, and revealed that discordant YAP1 and HER-2 expression may exist during the metastatic processes

Implications of all the available evidence

Microfluidic Chips developed in our study could not only rapidly detect label-free free GC cells in ascites and peritoneal lavages with high-throughput, they could also analyze ascites cancer cells at the single-cell level, improving peritoneal metastasis diagnosis and investigation of therapeutic targets.

Introduction

Gastric cancer (GC) is one of the most common cancers and represents the second most common cause of cancer deaths worldwide.[1] Although efforts have been made to improve its treatment, the prognosis for GC remains unsatisfactory, especially for patients suffering from peritoneal metastasis.[2,3] It is commonly believed that free cancer cells detach from primary tumors, implant in the abdominal cavity, and cause peritoneal metastasis.[4] Difficulty in diagnosing these early events has a large influence on the poor prognosis of peritoneal metastasis.[5] Collectively, the separation and identification of free cancer cells from the abdominal cavity plays a vital role in diagnosing peritoneal metastasis. In traditional clinical practice, cytological examinations were performed on ascites and peritoneal lavages to detect free cancer cells. However, this conventional method lacks sensitivity[3,6] due to the difficulty for pathologists to distinguish the small number of GC cells from the background cells.[7] In addition, GC cells have a similar tissue origin as some background cells such as mesothelial cells, limiting the usefulness of cell sorting methods such as CellSearch which rely on epithelial cell markers.[8] Thus, developing a label-free, high sensitivity, and high through-put diagnostic method to separate GC cells from ascites and peritoneal lavages is necessary. Meanwhile, since discordant molecular status is not rare in primary and metastatic cancer cells,[9,10] investigating the molecular expression status of cancer cells in the ascites could be helpful to uncover drivers of peritoneal metastasis and discover new therapeutic targets and strategies. For example, Yes-associated protein 1 (YAP1) and Human epidermal growth factor receptor 2 (HER-2) expression in ascites cancer cells is worthy of examination. YAP1 is a transcriptional coactivator that regulates organ size and proliferation.[11,12] It is a specific marker of ascites cancer cells and plays an important role in metastasis.[13,14] YAP1 might represent a novel therapeutic target, as GC peritoneal metastasis was attenuated when YAP1 was inhibited.[15] HER-2 is a transmembrane tyrosine kinase receptor and an important target for GC therapy.[16,17] Trastuzumab combined with chemotherapy has been shown to improve overall survival in patients with advanced HER-2 positive GC.[17] However, due to the lack of a sensitive strategy for collecting the limited cancer cells in the ascites, analyzing the molecular expression status of these free cancer cells remains challenging. Hence, a technique to analyze the molecular expression of separated GC cells in ascites and peritoneal lavages at the single-cell level is also needed.

The exploration of physical and chemical mechanisms has promoted the development of cell separation and identification techniques in cell biotechnology. In previous studies, the Raman technique was used to capture hepatic carcinoma cells from whole blood samples and to sort *Escherichia coli* from aqueous samples.[18,19] Device-based dielectrophoresis (DEP) can be used to isolate bone marrow-derived mesenchymal stem cells from a heterogeneous cell mixture and to select monocytes from whole blood samples.[20,21] Acoustic techniques have been used to separate U87 cancer cells from red blood cells and to sort prostate cancer cells from whole blood samples.[22,23] Separation of yeast cells and *Escherichia coli* has been achieved using optic tweezer technology.[24,25] Indeed, these techniques all play large roles in cell separation-related research. However, the DEP method has a relatively complex structure, which may affect its convenience; acoustic techniques may lead to cells dissolving, affecting subsequent cellular analysis; the laser used in optic tweezers may also injure cells with photodamage and affect further analyses; and the throughput of Raman techniques was insufficient for subsequent studies. To improve early diagnosis and advance therapeutic strategies for GC peritoneal metastasis, new methods are needed to separate label-free cancer cells from ascites and peritoneal lavages with high-throughput rapidly and to investigate the molecular status of the separated cancer cells at the single-cell level.

Microfluidic technology has developed rapidly in recent years, becoming a promising method for cell separation. For example, Lin et al. achieved label free isolation of circulating tumor cells and gene expression characterization using the "Labyrinth" microfluidic device.[26] Zeming et al. presented a microfluidic device that could effectively purify reticulocytes generated from *in vitro* erythroid culture.[27] Through the microstructure design of the chip and controlled fluid dynamics, cells with different sizes are subjected to different forces and can be separated within the chip. Dean flow fractionation (DFF) and Deterministic lateral displacement (DLD) are typical microfluidic techniques for separating mixed cells according to size. The DFF technique takes advantage of the inertial lift force and Dean drag force that act on cells of different sizes to achieve differential migration, thus realizing cell separation.[28] The DLD technique can precisely control the path of particles larger and smaller than the critical diameter (D_c) through the specific arrangement of columns in the channel to achieve separation.[29,30] Both DFF and DLD can separate cells label-freely.[27,28,31] Because of the relatively larger size of cancer cells compared to leukocytes and other background cells, numerous studies separating circulating tumor cells have been conducted using the DLD and DFF techniques.[32–36] However, most DLD chips are often used individually, and they can only allow fluid to flow into the chip at a low velocity[34,37] to prevent internal blockages.[38] This limits the wide clinical application of DLD technology. Meanwhile, whether these techniques can be used to isolate GC cells from patients' ascites and peritoneal lavages is untested. Additionally, little is known about the molecular expression of free cancer cells in ascites due to the limited cancer cell numbers and detection methods. Due to possible differences in molecular status between primary and metastatic lesions, analyzing the molecular expression of metastatic tissues could help improve therapies for GC patients.[39] It is of great significance to analyze the molecular expression of free cancer cells in ascites, necessitating the construction of an integrated analysis chip for downstream identification and analysis of cancer cells after separation.

In this study, we used an integrated microfluidic device (IMD) composed of a spiral chip (using the DFF technique) and a DLD chip to achieve rapid GC cell separation from ascites and peritoneal lavages. The DFF spiral chip performs an initial cell separation and enrichment process, greatly improving the concentration and purity of the cancer cells entering the DLD chip, making higher efficiency of the subsequent isolation possible and overcoming the disadvantages inherent to using DLD chips alone. Because of this, the fluid inflow rate of the IMD can reach 100 μL/min, enabling high-throughput cell screening and separation. Afterwards, separated cells were identified and analyzed using a single-cell trapping array-chip (SCTA-chip). We successfully isolated cancer cells from simulated peritoneal lavages containing 1/10,000 cancer cells and 12 complete GC ascites samples. Our devices may impact clinical practice by serving as an auxiliary method for clinical cytological testing. We then performed molecular detection of EpCAM, YAP1, HER-2, CD45, and cytological examination of the separated cancer cells at the single-cell level using a SCTA-chip. At last, we performed a serial YAP1 and HER-2 expression analysis in nontumorous adjacent tissues (NATs), primary cancer lesions, metastatic cancer tissues, and ascites cancer cells, and revealed that YAP1 and HER-2 can have discordant expression during the metastatic processes. The molecular expression signatures detected in single ascites cancer cells may provide new therapeutic targets and strategies for GC peritoneal metastasis.

Methods

Experimental instruments

Illustrations of the IMD are presented in Supplementary Fig. S1a. Cells and PBS were injected into the IMD using a Harvard PHD ULTRA syringe pump (Harvard Apparatus, USA). The flow rate of the IMD at the sample inlet was 100 μL/min, and the flow rate for PBS inlet 1 was 650 μL/min. The DLD components require a 1:1 flow rate ratio between the two inlets (DLD inlet and PBS inlet 2, Supplementary Fig. S1a). The flow rate of

the DLD sample inlet was the same as waste outlet 1, at 350 μL/min. Thus, we settled on a flow rate of 350 μL/min for PBS inlet 2 of the DLD. The height of the DFF component was 170 μm. Bright-field images were observed by a Leica DFC300FX inverted fluorescence microscope (Oskar-Barnack-Straße, Germany) equipped with a Leica DMC5400 color camera (Oskar-Barnack-Straße, Germany) and a high-speed pco.dimax cs1 camera (Kelheim, Germany). Fluorescence images were collected using confocal laser scanning microscopy (CLSM, Leica TCS SP8, Germany).

In 2006, Inglis et al.[40] developed the theoretical basis of DLD, and suggested that $Dc = 2\eta g\varepsilon$ ($\varepsilon = \Delta\lambda/\lambda$), where g is gap spacing between posts (30 μm in our manuscript), $\Delta\lambda$ is row shift distance (5 μm in our manuscript), λ is the center-to-center post spacing (60 μm in our manuscript), and η is a variable parameter to accommodate for non-uniform flow through the gap. The η value suggested by Inglis et al.[40] could be obtained from the parabolic flow curve (Fig. 3 of Reference 40). At the same time, Beech et al.[41] demonstrated another η value calculation method of $\eta = \sqrt{(N/3)}$, where $N = 1/\varepsilon$ (=12 in our manuscript). According to the calculation methods suggested by both Inglis et al. and Beech et al., the Dc of our design is around 10 μm.

Cell culture, mixture, and preparation

AGS and SNU-16 cells were purchased from ATCC (AGS: Cat# CRL-1739, RRID: CVCL_0139; SNU-16: Cat# CRL-5974, RRID: CVCL_0076). HGC-27 cells (Cat# TCHu 22, RRID: CVCL_1279) were purchased from the Institute of Biochemistry and Cell Biology at the Chinese Academy of Sciences.MKN-45 (Cat# KG323, RRID: CVCL_0434), SNU-5 (Cat# KG441, RRID: CVCL_0078), MKN-28 (Cat# KG605, RRID: CVCL_1416) and MKN-74 (Cat# KG528, RRID: CVCL_2791) cells were purchased from KeyGEN BioTECH.HGC-27, SNU-16, MKN-28, MKN-74 and AGS cells were cultured in RPMI 1640 medium with 10% fetal bovine serum (FBS). MKN-45 were cultured in DMEM/F12 medium with 10% FBS. SNU-5 was cultured in IMDM medium with 20% FBS. All cells were incubated in a humidified atmosphere with 37 °C and 5% CO_2. The adherent cells (HGC-27, AGS, MKN-28, MKN-74 and MKN-45) were digested with trypsin when the cell density reached 80%–90% then collected by centrifugation at 1000 rpm for 2 min. Cell density and diameter were determined via Scepter 2.0 Handheld Automated Cell Counter (Millipore, USA). Mycoplasma screening for cell lines was performed monthly to exclude mycoplasma contamination by Mycoplasma Detection Kit (Beyotime, China). The screening results was found to be all negative. All the cell lines were validated and relative files are shown in Reagent Validation file as Supplementary material.

For cell mixtures, HGC-27 cells were labeled with fluorescent CellTracker Green CMFDA (C2925, Thermo Fisher Scientific, USA) in serum-free medium at 37 °C for 30 min, washed twice with phosphate-buffered saline (PBS; Invitrogen, USA), then recovered in complete medium for 30 min. The HGC-27 cells were then digested using trypsin (Invitrogen, USA) then mixed with hysteromyoma lavage cells. Corresponding numbers of fluorescently labeled HGC-27 cells were added to lavage cells at different ratios and mixed well using pipettes. For ratios of 1:10, 1:100, 1:1000 and 1:10,000 (cancer cells: hysteromyoma lavage cells), 1×10^5, 10,000, 1000, or 100 HGC-27 cells were added to 1×10^6 hysteromyoma lavage cells, respectively.

Ethical approval

All procedures performed in studies involving human participants were in accordance with the ethical standards of the institutional research committee and with the 1964 Helsinki declaration and its later amendments or comparable ethical standards. Ascites and lavage fluids were collected after obtaining informed consent from patients in accordance with institutional ethical guidelines, which were reviewed and approved by the Research Ethics Committee of First Hospital of China Medical University (2019-231, Shenyang, China).

Clinical samples collection and preparation

Ascites was obtained from patients with GC admitted to the First Hospital of China Medical University. Three peritoneal lavage fluid samples were also collected from patients with hysteromyoma who underwent abdominal surgery in the First Hospital of China Medical University. Sex was self-reported by study participants. Ascites and hysteromyoma lavages were centrifuged at 1000 g for 10 min, then pelleted cells were stored at −80 °C until further use. When performing cell separation, cells were filtered with a 40 μm filter element to remove impurities in the ascites which may influence cell separation then fixed with 4% paraformaldehyde (Biosharp, Anhui, China) for 10 min. Finally, the cells were suspended in PBS and added to microfluidic chips.

Single-cell in situ immunofluorescence on a chip

Cells were loaded into the SCTA-chip at a flow rate of 12 μL/min. Cells were permeabilized with 0.1% Triton X-100 (Shanghai Beyotime Biotechnology Co. Ltd., China) for 5 min then blocked with 1% BSA (Solarbio, China) at 37 °C for 1 h. Next, the cells were incubated with 25 μL HER-2 aptamer (200 nM, Sangon Biotech, China) and Anti-YAP1 (1/200, Boster, USA, RRID: AB_2921202) and Anti-CD45 (1/150, Immunoway, USA, RRID: AB_2921203) antibodies at 37 °C for 30 min, then washed with PBS. After that, 25 μL Alexa Fluor® 647 (1/500, ab150075, Abcam, USA, RRID: AB_2752244), Alexa Fluor® 488-Anti-EpCAM (1/100, ab237395, Abcam, RRID: AB_2921205), and Alexa Fluor® 405 (1/500, ab175660, Abcam, RRID: AB_2885184) were infused into the chip and incubated with

cells at 37 °C for 30 min, then washed with PBS. Finally, fluorescence imaging of the cells was carried out using CLSM at four excitation wavelengths (405, 488, 561 and 633 nm), with corresponding emission wavelengths collected at 420–500, 500–560, 570–650, and 650–720 nm, respectively. When performing immunefluorescence co-localization of HER-2 aptamer with HER-2 antibody, Alexa Fluor® 488 Anti-HER-2 antibody (1/100, ab225509, Abcam, RRID: AB_2922429) and 25 μL HER-2 aptamer (200 nM, Sangon Biotech, China) were utilized for analysis.

Single-cell in situ Wright-Giemsa staining on a chip

The cell suspension was injected into the SCTA-chip at 12 μL/min. Wright-Giemsa staining was done with Wright-Giemsa stain kits (BA-4017, BASO, China) according to the manufacturer's instructions. In brief, 20 μL Wright-Giemsa staining solution A was infused into the chip to stain for 1 min. After that, a mixed solution of A and B (1:2) was passed into the chip for 3 min.

ThinPrep papanicolaou staining

The ascites samples separated by IMD were added into 20 mL Thinprep PreservCyt solution (70787–004, Hologic, USA). Slides were prepared using the ThinPrep 2000 Processor (Hologic, USA) and stained with the standard Papanicolaou staining method according to the manufacturer's instructions.

Conventional Wright-Giemsa staining

According to the manufacturer's instructions, conventional Wright-Giemsa staining was performed by the Wright-Giemsa stain kit (BA-4017, BASO, China). Briefly, cells were smeared on adhesive slides and dried for 10 min. Then, 0.5 mL Wright-Giemsa staining solution A was added to the slide and stained for 1 min. Then, 1 mL of solution B was added to solution A, blown with an aurilave to mix the solutions well, and stained for 4 min. Then, the slides were washed by distilled water, and dried at room temperature. At last, we fixed the slides by neutral balsam.

Immunohistochemistry

Tissue samples were mixed in 4% formaldehyde, embedded in paraffin, and sectioned at a thickness of 5 μm. Tissue sections were deparaffinized in xylene and rehydrated with descending concentrations of ethanol. After blocking with endogenous peroxidase, tissue sections were incubated with primary antibodies against YAP1 (ab52771, Abcam, RRID: AB_2219141) and HER-2 (790-4493, Ventana, RRID: AB_2921204) overnight at 4 °C. The sections were then incubated with secondary antibody for 1 h and washed with PBST. A diluted 3, 3′-diaminobenzidine was added as a substrate for staining in the dark and counterstained with hematoxylin. Pathologists evaluated the results.

Analysis of recovery rate and purity

After IMD separation, the recovery rate and purity of the cancer cell line cells and simulated samples were calculated using Formula 1 and Formula 2, respectively. N1 represented the number of cancer cells collected from the cancer outlet of the IMD. N2 was the number of cancer cells collected from waste outlet 1 of the DFF chip. N3 was the number of cancer cells collected from waste outlet 2 of the DLD chip. N4 was the total number of cells collected from the tumor outlet of the IMD. The cell capture rate of the SCTA-chip was calculated by Formula 3, where N5 was the number of cells captured by the SCTA-chip and N6 was the total number of cells that entered the SCTA-chip.

$$\text{Recovery rate} = \frac{N1}{N1+N2+N3} \times 100\% \qquad \text{Formula 1}$$

$$\text{Purity} = \frac{N1}{N4} \times 100\% \qquad \text{Formula 2}$$

$$\text{Capture rate} = \frac{N5}{N6} \times 100\% \qquad \text{Formula 3}$$

For clinical ascites samples, the separated cells in the SCTA-chip were stained by the Wright-Giemsa method to confirm the separation accuracy. Five visual fields were selected randomly, and cells were identified by pathologists. We then calculated the proportion of cancer cells present in the total separated cells (referred to as purity) in the selected visual fields for each sample. For separated cells stained by conventional Wright-Giemsa staining, we also selected five random visual fields and calculated the proportion of cancer cells present in the total cells.

Pooled analysis of overall purity

The overall purity of the cancer cell separation in ascites samples was analyzed through pooled analysis by Stata software, version 12.0 (Stata Corp, College Station, TX, USA). Three commands were used as followed: (1) gen R = n/N, (2) gen ser = sqrt (R*(1 – R)/N), (3) metan R ser, fixed. In command (1), R is the purity of one sample, n refers to the number of cancer cells, and N is the number of total separated cells. In command (2), ser refers to the SE of the purity. Stata software will analyze the overall purity according to command (3).

Statistical analysis

All statistical analyses were conducted using SPSS 20.0 software (IBM Corp, USA). The data is listed as mean ± standard deviation. The difference between two groups was analyzed by t-test. $P < 0.05$ is considered significant.

Role of funders
The funders were not involved in the study design, data collection, data Formal analysis, interpretation, or writing of report.

Results

Separation of cancer cell basing on hydrodynamics

The main steps of the experiment are shown in Fig. 1. First, doctors collected patients' ascites and peritoneal lavages during cancer examinations or treatments. The collected ascites contained a large number of peritoneal mesothelial cells and immune cells, but only few GC cells. Cells from the samples were injected into the IMD and first passed through the spiral chip. Different sized cells were focused at different positions of the spiral chip under the inertial lift force and Dean drag force. Cells of smaller sizes, such as mesothelial cells and immune cells, were focused at the outside of the channel and flowed out of waste outlet 1 of the spiral channel. Cells of larger sizes, such as GC cells, were focused on the inside of the channel and then entered the DLD chip. According to the DLD principle, cells larger than D_c (10 μm) were deflected to the cancer outlet, while smaller cells followed the original flow direction and flowed out waste outlet 2. For high sensitivity and high-throughput identification of the selected cells, the cells collected from the cancer outlet were pumped into the SCTA-chip, which was specially designed to collect cancer cells. Cells were captured by a single cell trap with a width of 25 μm and a minimum gap of 8 μm. When a cell trap was occupied, other cells flowed to unoccupied single cell traps, forming an ordered single cell array in a short period of time. Using the SCTA-chip, EpCAM, YAP1 and HER-2 expression were detected in situ via immunofluorescence imaging to determine molecular expression of separated cells. Following that, the separated cells in the SCTA-chip were stained by the Wright-Giemsa method to calculate separation accuracy.

Separation efficiency of cell line samples in IMD and imaging in the SCTA-chip

Illustrations of the IMD and SCTA-chip are presented in Supplementary Fig. S1. To verify whether our device could separate cancer cells, we measured the diameter of seven GC cell lines (HGC-27, SNU-16, MKN-45, AGS, SNU-5, MKN-28, and MKN-74) and three hysteromyoma lavage cells (H1–H3), which did not contain cancer cells. As indicated in Supplementary Fig. S2, the cancer cell lines were all larger than 10 μm in diameter (17.37 μm for HGC-27, 17.02 μm for SNU-16, 19.10 μm for MKN-45, 17.54 μm for AGS, 21.74 μm for SNU-5, 18.42 μm for MKN-28, and 15.98 μm for MKN-74), and the hysteromyoma lavage cells were smaller than 10 μm in diameter (7.14 μm, 7.71 μm, and 8.53 μm for three samples), laying the foundation for isolating cancer cells via IMD. Then, we compared recovery rates of 100 HGC-27 cells at different IMD sample inlet speeds. At speeds of 50, 100, 150, and 200 μL/min, the recovery rates were 76.97 ± 1.65%, 81.52 ± 0.94%, 78.22 ± 0.95%,

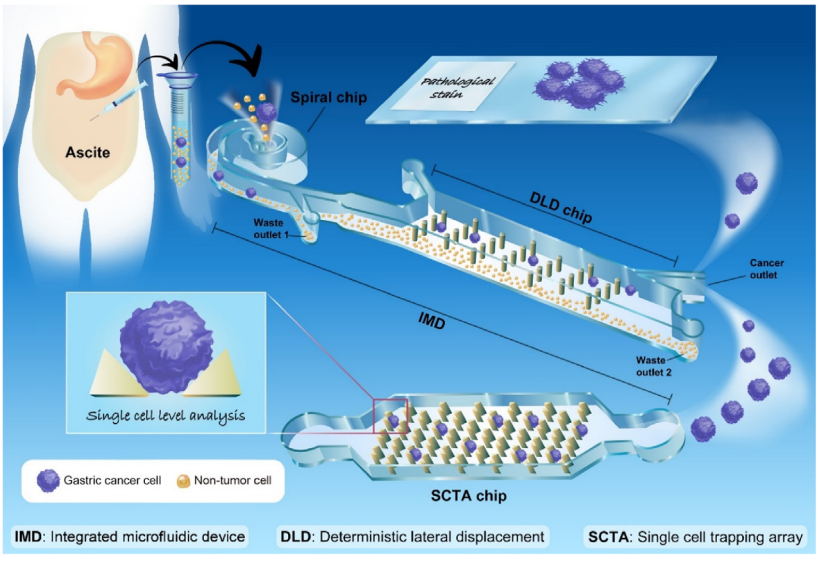

Fig. 1: **The device based on microfluidic techniques developed for separating cancer cells from ascites and further analysis at the single cell level.** Ascites obtained from patients are placed in the integrated microfluidic device (IMD) composed of a spiral chip (using the Dean Flow fractionation (DFF) technique) and a Deterministic lateral displacement (DLD) chip. Gastric cancer cells with larger relative size can be separated from ascites. A portion of the separated cells can be stained for pathological identification, with the rest of the separated cells being stained and analyzed at the single-cell level in the single-cell trapping array-chip (SCTA-chip).

and 79.11 ± 1.49%, respectively. Therefore, we chose 100 μL/min for further studies. Moreover, to calculate the recovery rate of the IMD, different numbers of cancer cells (50, 100, 500 cells) were injected into the device inlet. As shown in Fig. 2a, recovery rates for the different types and numbers of tumor cells were above 80%.

To test whether our SCTA-chip could achieve high-efficiency cell capture, we used AGS cells to verify the SCTA cell capture rate, finding that the capture rate could reach 95% (Fig. 2b), demonstrating high-throughput and efficient capture of cancer cells separated from ascites. Subsequently, to provide theoretical support for the design of the SCTA chip and the hydrodynamics of samples within the chip, we performed a finite element analysis using COMSOL Multiphysics. As shown in Fig. 2c–d, the surface velocity distribution and streamlines plots demonstrate that the fluidic streamlines are compressed in a compact configuration between the traps but are sparse within the traps. As a result, the flow slows down at the trap area but speeds up between the traps. Therefore, cells could be captured in the traps either when they travel along streamlines which transverse open traps or when they come close enough to be drawn into the trap. We next tested cell loss during the exportation of enriched cells from the IMD to the SCTA-chip. We transferred about 50 collected cells from the IMD to the SCTA-chip and successfully trapped 36 ± 6 cells in the SCTA chip.

Moreover, we analyzed four-color immunofluorescence imaging and Wright-Giemsa staining of AGS cells on the SCTA-chip, as shown in Fig. 2e. Immunofluorescence results showed that AGS cells were EpCAM$^+$/YAP1$^+$/HER-2$^+$/CD45$^-$. Wright-Giemsa staining in the

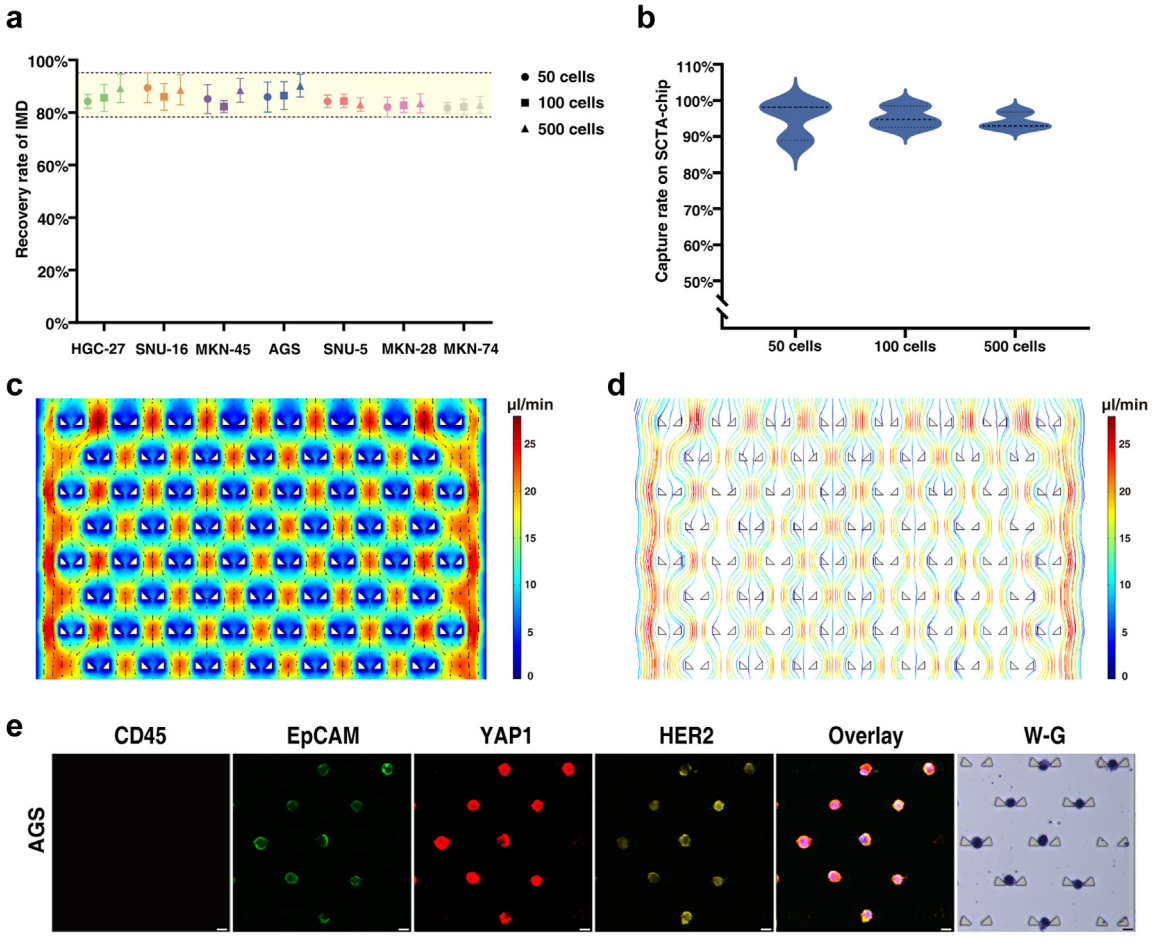

Fig. 2: **IMD for separating cancer cells and SCTA-chip for identifying cancer cells.** (a) Recovery rates of seven cancer cell lines at different numbers of cells (n = 9 for each cell line). (b) Capture rate of AGS cells at different numbers. (c) Finite element analysis using COMSOL Multiphysics for the SCTA chip: flow velocity distribution on the chip. (d) Finite element analysis using COMSOL Multiphysics for the SCTA chip: flow velocity streamlines on the chip. (e) Confocal fluorescence images of CD45/EpCAM/YAP1/HER-2 and Wright-Giemsa staining of AGS cells on the SCTA-chip. Scale bar, 8 μm (The minimum gap of a single cell trap, 8 μm).

SCTA chip showed that AGS cells were hyperchromatic with large nuclei, consistent with Wright-Giemsa staining results using the conventional method (Supplementary Fig. S3). Furthermore, we calculated cell loss after immunofluorescence and Wright-Giemsa staining in the SCTA-chip to determine whether the SCTA-chip can help avoid cell loss during staining (Supplementary Fig. S4). We followed 100 SCTA-chip trapped cells before staining. After immunofluorescence, all 100 cells remained in the chip, and 95 cells still remained after Wright-Giemsa staining in the chip. At last, to confirm the binding specificity of HER-2 aptamer, we performed immune-fluorescence co-localization of the HER-2 aptamer with HER-2 antibody on AGS cells inside the SCTA-chip (Supplementary Fig. S5). The results showed that the immunofluorescence of the HER-2 aptamer (yellow) had the same location as the HER-2 antibody (green).

Evaluation of IMD in separating simulated samples

To simulate mixtures of GC cells within ascites or peritoneal lavage cells, we mixed HGC-27 GC cells with hysteromyoma lavage cells in proportions of 1:10, 1:100, 1:1000 or 1:10,000. The cancer cells were incubated with CellTracker Green 5-Chloromethylfluorescein Diacetate (CMFDA) prior to mixing, allowing us to identify cancer cells via fluorescence microscopy before and after separation. In the first stage of separation, most of the hysteromyoma lavage cells were sorted away from the cancer cells and flowed out of waste outlet 1, while cancer cells flowed through the inner outlet to enter the DLD channel with some remaining hysteromyoma lavage cells (Fig. 3a, Supplementary Movie S1). In the second stage, the larger cancer cells were deflected to the cancer outlet while the smaller hysteromyoma lavage cells flowed out of waste outlet 2 (Fig. 3b, Supplementary Movie S1). By counting the number of cancer cells and lavage cells at the final collection outlet, the recovery and purity of the isolated samples could be calculated. For samples with cell ratios of 1:10, 1:100, 1:1000 and 1:10,000, the recovery rates were 86.6 ± 8.49%, 88.6 ± 1.34%, 94.5 ± 4.24% and 84.8 ± 9.11% respectively, and the purity rates were 78.8 ± 2.33%, 82.0 ± 4.88%, 67.6 ± 1.20% and 72.4 ± 3.78% respectively (Fig. 3c). As shown in Supplementary Fig. S6, background cells were significantly reduced after sorting. After sorting the samples containing fluorescently stained cancer cells, the isolated cells acquired from the cancer outlet were injected into the inlet of the SCTA-chip, stained using the Wright-Giemsa method, then observed under a microscope. The separated cells were hyperchromatic with large nuclei, and the cell morphology of HGC-27 cells Wright-Giemsa stained using the conventional method was used for contrast (Supplementary Fig. S7). In this way, we could validate the cells were truly cancer cells. Images of cancer cells after separation from the four simulated samples are presented in Fig. 3d. To further evaluate the superiority of integrating the DFF and DLD techniques together, we further compared IMD with individual DFF or DLD devices to compare recovery rates and purity of cell separation in simulated lavage samples (HGC-27 GC cells with hysteromyoma lavage cells in proportions of 1:100). The results showed that the recovery rate and purity of separation were 57.63 ± 4.47% and 57.22 ± 6.46%, respectively, for the individual DFF device and 60.21 ± 5.27% and 58.15 ± 2.76% for the individual DLD device. The integrated microfluidic device (combined DFF and DLD technique) showed a higher recovery rate (88.6 ± 1.34%) and purity (82.0 ± 4.88%) than either individual DFF or DLD device.

Separation and analysis of cancer cells from patients' ascites

To trial our method with actual GC samples, we separated cancer cells from complete GC ascites samples from 12 patients (P01–P12). Basic patient information is shown in Table 1. Samples were separated by IMD at a speed of 100 μL/min. Afterwards, as is performed in the clinic, some of the separated cells were stained using the ThinPrep Papanicolaou method. Microscopic images of the samples before and after separation are presented in Supplementary Fig. S8. This demonstrated that our device could concentrate cancer cells with high throughput, making it easier for pathologists to find cancer cells in ascites by excluding a large amount of background cells.

The rest of the separated cells were injected into a SCTA-chip for further analysis. To prove that the separated cells were cancer cells, expression of EpCAM, YAP1, and CD45 were analyzed using in situ immunofluorescence. As a marker of epithelial cells, EpCAM is a classic tumor cell marker[42,43]; YAP1 was chosen for its use as a tumor cell marker in ascites with certain specificity[15]; and CD45 was selected to exclude immune cells.[44,45] Separated cells from all samples showed $EpCAM^+/CD45^-$ expression. Moreover, cells separated from P02, P03, P04, P05, P06, P07, P08, P10, P11, and P12 showed $EpCAM^+/YAP1^+/CD45^-$ expression (Fig. 4a). We also stained separated non-cancer cells from the waste outlets of six ascites samples to provide a comparison (Supplementary Fig. S9). The results showed positive CD45 expression in some cells while EpCAM, YAP1, and HER-2 had negative expression in almost all the cells.

After immunofluorescence imaging, the separated cells from the SCTA-chip were stained by the Wright-Giemsa method to further confirm the separation accuracy. Pathologists identified the separated cells as mostly hyperchromatic with large nuclei, consistent with the characteristics of cancer cells (Fig. 4b). The Wright-Giemsa staining results could also verify cells in

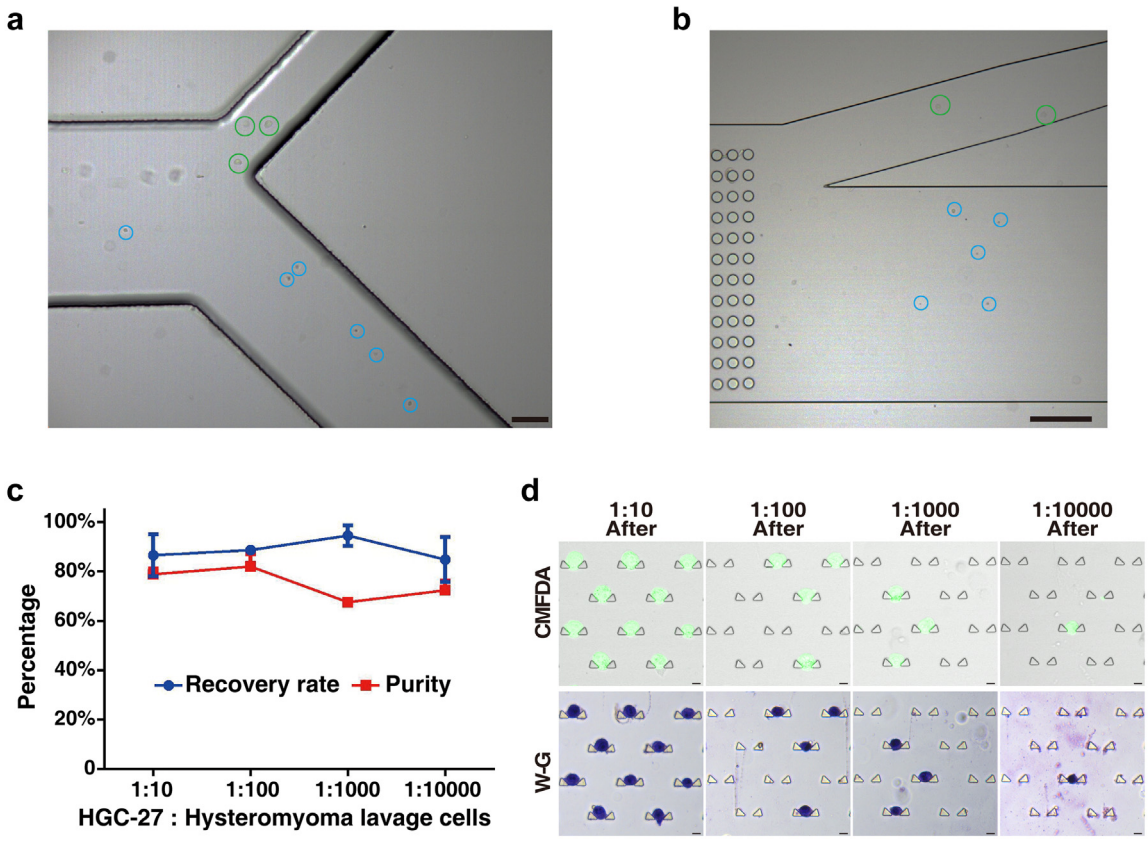

***Fig. 3:* Separation and evaluation of simulated samples.** (a) Representative images of cells at the spiral outlet of IMD. Most of the hysteromyoma lavage cells with smaller size (in blue circle) were sorted from cancer cells and flowed out of the waste outlet 1, while larger cancer cells (in green circle) flowed through inner outlet with some hysteromyoma lavage cells and then entered DLD channel. Scale bar, 100 μm. (b) Representative images of cells at the DLD outlet of IMD. Cancer cells with larger size (in green circle) were deflected to the cancer outlet, while smaller hysteromyoma lavage cells (in blue circle) flowed out of the waste outlet 2. Scale bar, 100 μm. (c) Recovery and purity of simulated samples. (d) Fluorescence images of separated cancer cells in the SCTA-chip. Scale bar, 8 μm (The minimum gap of a single cell trap, 8 μm).

SCTA chip were intact ones (Fig. 4a and b). We then calculated the separation purity (proportion of cancer cells present in the total separated cells in five randomly selected visual fields) in each sample. For the 12 samples analyzed, the purity of 8 samples were higher than 70%, the purity of 2 were higher than 80%, and the highest purity was 86% for P06 with 51 cells identified as cancer cells in a total of 59 cells. The detailed information of separation purity is shown in Table 1. Moreover, the overall purity of the cell separation was analyzed through a pooled analysis method using Stata software, finding an overall purity of 73% (Fig. 4c). Moreover, we also performed conventional Wright-Giemsa staining on separated cancer cells from P06, P07, and P11 (Supplementary Fig. S10). The purity was 83.3% (20/24) for P06, 61.3% (19/31) for P07, and 65.1% (41/63) for P11, which show no significant difference (P = 0.98 by paired t test) compared with Wright-Giemsa staining of the same samples inside the SCTA-chip.

Serial analysis of YAP1 expression in tissues and ascites cancer cells

Besides ascites samples, we also collected primary cancer lesions from 6 patients (P04, P05, P06, P07, P08, P09), as well as NATs and metastatic lymph node/tumor deposits (TD) from 4 patients (P04, P05, P06, P07). In our study, metastatic lymph nodes (P05 and P06) and TD (P04 and P07) represented metastatic tissues for GC. We performed a serial analysis of YAP1 expression, finding different YAP1 expression patterns among each patient (Fig. 5).

The tissues from P04 and P07 were collected when the patient received palliative surgery. The tissues from P05 and P06 were collected when the patient received radical surgery before ascites occurred. We summarized the serial analysis results of Yap1 expression pattern in Supplementary Table S1. The IHC score of NAT, primary lesion and metastatic lymph nodes/TD were “1, 2, and 2 for P04”; “3, 1, and 3 for P05”; “2, 2, and 2 for P06”; “1, 3, and 3 for P07”. Same as shown above,

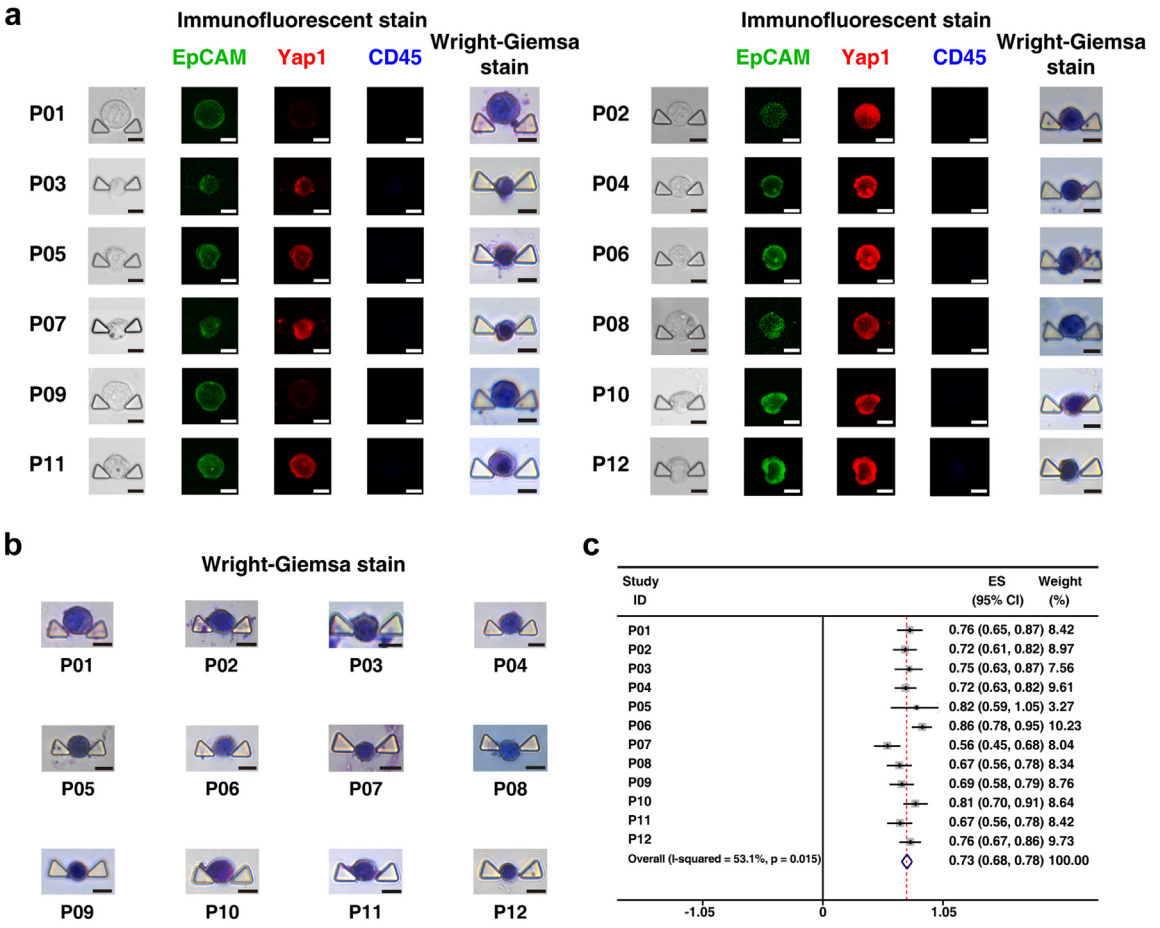

***Fig. 4:* Separation and analysis of cancer cells from patients' ascites.** (a) Three-color immunofluorescence imaging and Wright-Giemsa staining in the SCTA-chip for separated cells from 12 ascites samples. Scale bar, 8 μm (The minimum gap of a single cell trap, 8 μm). (b) Wright-Giemsa staining for separated cells in the SCTA-chip. Scale bar, 8 μm (The minimum gap of a single cell trap, 8 μm). (c) The overall purity analysis of cell separation based on Wright-Giemsa staining results.

Patient	Sex[a]	Age	Primary lesions position	Cell volume before separation	Histological type	Separation purity calculation[b]		
						Purity	Identified as cancer cells	Total cells
P01	M	62	Gastric horn	5×10^6 cells in 5 mL	Adenocarcinoma	76%	44	58
P02	F	30	Lesser curvature of gastric body	1×10^6 cells in 3 mL	Mucinous adenocarcinoma	72%	53	74
P03	M	72	Gastric antrum	1×10^6 cells in 3 mL	Adenocarcinoma	75%	36	48
P04	F	27	Gastric antrum	1×10^6 cells in 4 mL	Adenocarcinoma	72%	62	86
P05	M	32	Gastric horn	2×10^6 cells in 4 mL	Adenocarcinoma	82%	9	11
P06	F	68	Lesser curvature of gastric body	4×10^6 cells in 4 mL	Adenocarcinoma	86%	51	59
P07	F	66	Gastric antrum	3×10^6 cells in 5 mL	Adenocarcinoma	56%	40	71
P08	M	78	Gastric antrum	3×10^6 cells in 5 mL	Adenocarcinoma	67%	46	69
P09	F	45	Lesser curvature of gastric body	1×10^6 cells in 5 mL	Adenocarcinoma	69%	51	74
P10	M	65	Gastric antrum	2×10^6 cells in 5 mL	Mucinous adenocarcinoma	81%	42	52
P11	F	64	Posterior wall of gastric body	2×10^6 cells in 4 mL	Adenocarcinoma	67%	47	70
P12	F	56	Greater curvature of gastric body	2×10^6 cells in 4 mL	Signet-ring cell carcinoma	76%	61	80

[a]M for male and F for female. [b]The proportion of cancer cells present in the total cells. Cancer cells were identified by pathologist.

***Table 1:* Basic information and separation purity of patients.**

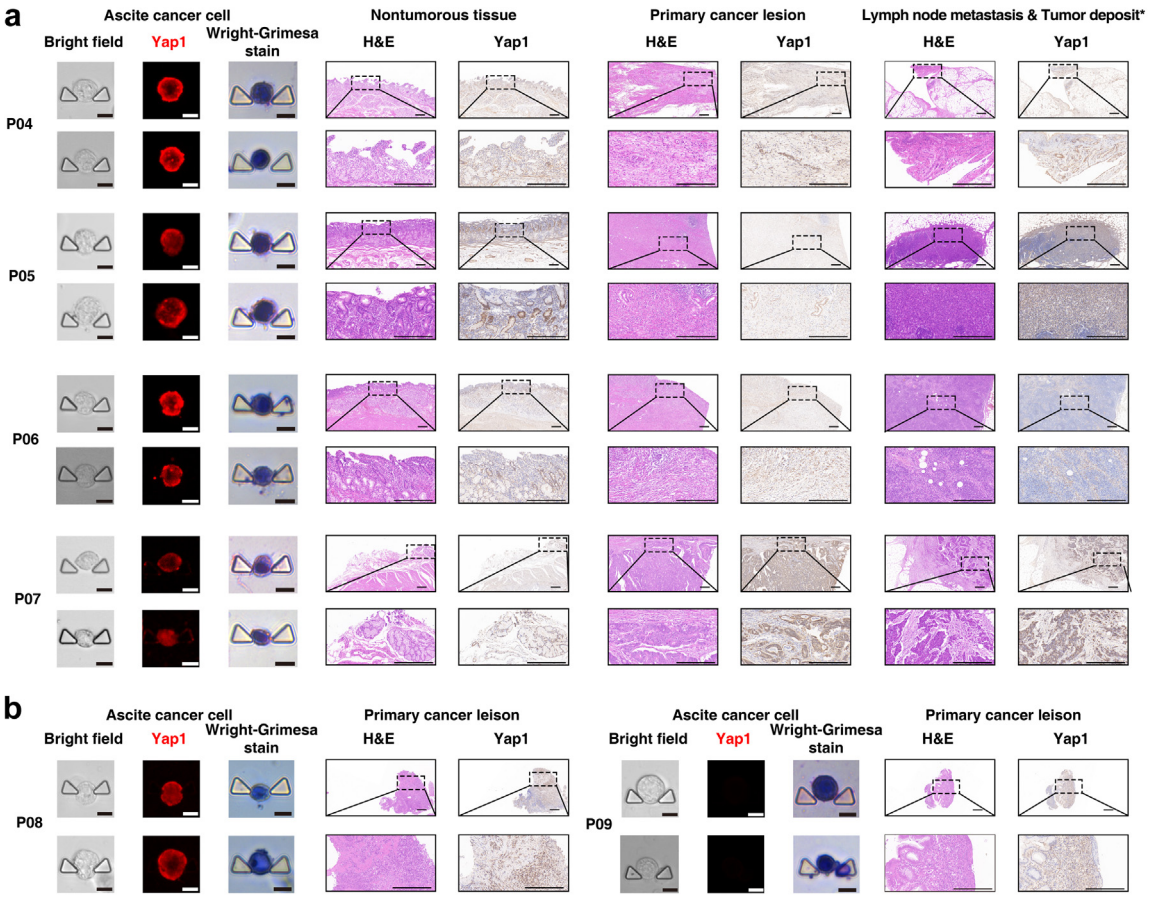

***Fig. 5:* Serial analysis of YAP1 expression in tissues and ascites cancer cells.** (a) YAP1 expression and Wright-Giemsa staining in NATs, primary cancer lesions, lymph node metastasis/TD, and ascites cancer cells for P04–P07. *TD for P04 and P07; Lymph node metastasis for P05 and P06. (b) YAP1 expression and Wright-Giemsa staining in primary cancer lesions and ascites cancer cells for P08 and P09. Expression in tissues (NATs, primary cancer lesions, and lymph node metastasis/TD) were analyzed by IHC, Scale bar, 300 μm. Expression in ascites cancer cells was analyzed by in situ immunofluorescence, Scale bar, 8 μm (The minimum gap of a single cell trap, 8 μm).

P04–P07 all had positive YAP1 expression in ascites cancer cells (Fig. 5a). For P08 and P09, primary lesion tissues were collected when the patients received endoscopic examination. The expression score of YAP1 was 2 in both tissues, with YAP1 positively expressed in ascites cancer cells from P08, but negative in P09 (Fig. 5b).

Serial analysis of HER-2 expression in tissues and ascites cancer cells

HER-2, a key oncogene and driver of tumorigenesis, is an important treatment biomarker for targeted therapy in many human cancers.[16,46] In GC, trastuzumab plus chemotherapy have become the first-line treatment regimen for HER-2 positive advanced cancer.[17]

Thus, we examined HER-2 expression in IMD-separated cancer cells using the SCTA-chip and in situ immunofluorescence. HER-2 was positively expressed in separated cancer cells from eight patients (P02, P03, P05, P08, P09, P10, P11, and P12), with negative expression in the separated cancer cells from the other four (P01, P04, P06, P07). In summary, 8 out of 12 samples showed positive HER-2 expression.

Following the cellular analysis, we also performed a serial analysis of HER-2 expression in tissue samples, and compared HER-2 expression between primary and metastatic GC tissues or cells. We also summarized the serial analysis results of HER-2 expression pattern in Supplementary Table S1. P04 and P06 had negative HER-2 expression in the all tissues or cells (Fig. 6a). For P05 and P07, HER-2 was both positive expressed in ascites cancer cells, and the IHC score of NAT, primary lesion and metastatic lymph nodes/TD were "0, 0, and 2 for P05"; "0, 1, and 1 for P07" (Fig. 6a). Moreover, HER-2 was positively expressed in ascites cancer cells of both P08 and P09, with primary lesion expression scores of 3 in P08 and 1 in P09 (Fig. 6b). HER-2 tissue expression was further verified by IHF. The results were similar to

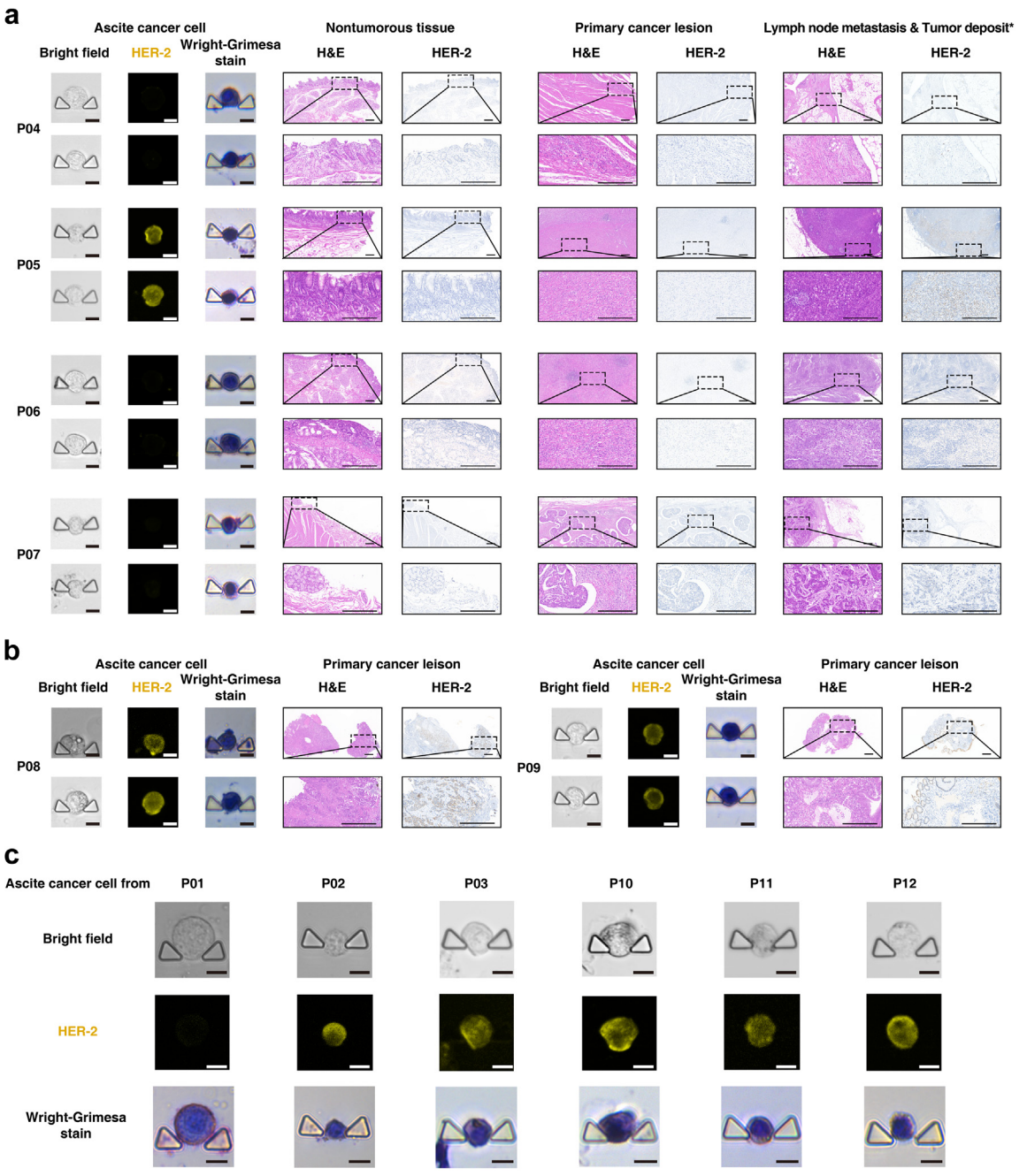

***Fig. 6:* Serial analysis of HER-2 expression in tissues and ascites cancer cells.** (a) HER-2 expression and Wright-Giemsa staining in NATs, primary cancer lesions, lymph node metastasis/TD, and ascites cancer cells for P04–P07. *TD for P04 and P07; Lymph node metastasis for P05 and P06. (b) HER-2 expression and Wright-Giemsa staining in primary cancer lesions and ascites cancer cells for P08 and P09. (c) HER-2 and Wright-Giemsa staining in ascites cancer cells for P01, P02, P03, P10, P11, and P12. Expression in tissues (NATs, primary cancer lesions, and lymph node metastasis/TD) analyzed by IHC, scale bar, 300 μm; Expression in ascites cancer cells analyzed by in situ immunofluorescence, Scale bar, 8 μm (The minimum gap of a single cell trap, 8 μm).

IHC, with positive HER-2 expression in the primary lesions of P07, P08, and P09, the metastatic lymph node of P05, and the TD of P07 (Supplementary Fig. S11).

The ability of our devices in separating and analyzing living cells

For above experiments in our manuscript, we fixed all cells with paraformaldehyde (instead of using living cells) because the 12 ascites samples were from our biobank collection stored at –80 °C. Since freeze-thawed unfixed cells are weaker than fresh cells or fixed cells, using living cells may have resulted in the cells breaking into fragments during the separation and analysis processes in the microfluidic chips. Thus, we fixed the ascites cells to enhance the success rate and achieve cancer cell separation in all 12 clinical ascites samples.

Therefore, we next tested the ability of our devices to separate and analyze living cells. We injected HGC-27 cells into the IMD and performed Live-Dead Cell Staining on the collected cells in the cancer outlet. We found that almost all cells were alive (Fig. 7a). Afterwards, we added unstained collected HGC-27 cells into the SCTA chip and again found almost all of the cells in the SCTA chip were alive. The cells in the SCTA chip were also validated by Wright-Giemsa staining at the single cell level, which showed that the cells were hyperchromatic, with large nuclei indicating that the cells were cancer cells (Fig. 7b). Furthermore, we mixed live HGC-27 GC cells with fresh peritoneal lavage cells in a 1:10 proportion. The cancer cells were incubated with CMFDA prior to mixing. We injected this live cell mixture (HGC-27: peritoneal lavage cells = 1:10) into the IMD. As shown in Fig. 7c, background cells were significantly reduced after sorting. The recovery and purity rates were 79.08 ± 2.69% and 77.99 ± 3.19%, respectively, with no significant difference seen when comparing with fixed cells ($P = 0.42$ by student's t-test for recovery rate, $P = 0.77$ by student's t-test for purity rate; the recovery rate and purity of fixed cells were 86.6 ± 8.49% and 78.8 ± 2.33%, respectively, as shown previously). Separated cells were also injected into the SCTA chip then Wright-Giemsa staining performed to verify cancer cell identity at the single cell level. The results showed that the cells were hyperchromatic, with large nuclei indicating that the cells were cancer cells (Fig. 7d).

Discussion

Early diagnosis of peritoneal metastasis is essential for improving prognosis of patients with GC. Separating and enriching cancer cells from ascites and peritoneal lavages can improve the sensitivity and convenience of traditional clinical cytological examinations. But separating cancer cells from the large amount of background cells with high throughput and high purity still presents a difficult problem. This shortcoming hinders further single-cell analysis of free cancer cells in ascites and peritoneal lavages, impeding the identification of new therapeutic targets. Therefore, new methods to separate cancer cells are urgently needed, both to improve early diagnosis of peritoneal metastasis and to allow for analysis of single free cancer cells in ascites and peritoneal lavages to promote the development of treatments for peritoneal metastasis.

In this paper, we introduce a new method to improve early diagnosis of peritoneal metastasis based on an integrated microfluidic chip combining DFF and DLD principles. DFF and DLD show complementary advantages. The DFF technique takes advantage of the inertial lift force and Dean drag force that act on cells of different sizes to achieve differential migration and realize cell separation. This cell separation method based on inertial force has the advantage of being label-free, high speed, and high throughput. However, when sorting cells in bodily fluids, the interaction between cells seriously affects their focusing behavior due to the complex body fluid environment and the interference of background cells, so sorting purity is relatively low. The DLD technique can precisely control the path of particles larger and smaller than the critical diameter (Dc) through the specific arrangement of columns within the channel to achieve separation. However, liquid flow is limited by the microcolumn in the DLD chip, and the throughput of this technique is relatively low. By combining these two techniques with the DFF chip at the prime site, our method achieves label-free, high-throughput, and high-purity cell separation of cancer cells from ascites and peritoneal lavages. Subsequently, we successful analyzed EpCAM, YAP1, and HER-2 expression of ascites cancer cells at the single cell level using the SCTA-chip. On this basis, we further explored the expression pattern of YAP1 and HER-2 in NATs, primary cancer lesions, TD, and metastatic lymph nodes. The results revealed that most ascites cancer cells and metastatic lesions showed similar YAP1 and HER-2 expression as the primary lesion, but expression of these genes may change during the metastatic process.

In our manuscript, we designed progressive experiments to verify our device's ability to separate cancer cells from ascites and peritoneal lavages. In the IMD device, the purpose of the DLD chip was to enhance purity without losing cancer cells that had already been separated by DFF. Thus, the DLD should have a relatively lower Dc. Therefore, we set the Dc of the DLD chip to 10 μm, as shown in the Methods, which was relatively lower than the DFF chip, whose Dc was near 12 μm (0.07 × channel height) in theory as shown by Warkiani et al.[35] We began by measuring cell size in seven GC cell lines and three hysteromyoma lavage cell samples. We found the average diameters of cancer cell lines were larger than Dc, and the diameters of hysteromyoma lavage cells were less than Dc. This provided the theoretical basis for cell separation using an

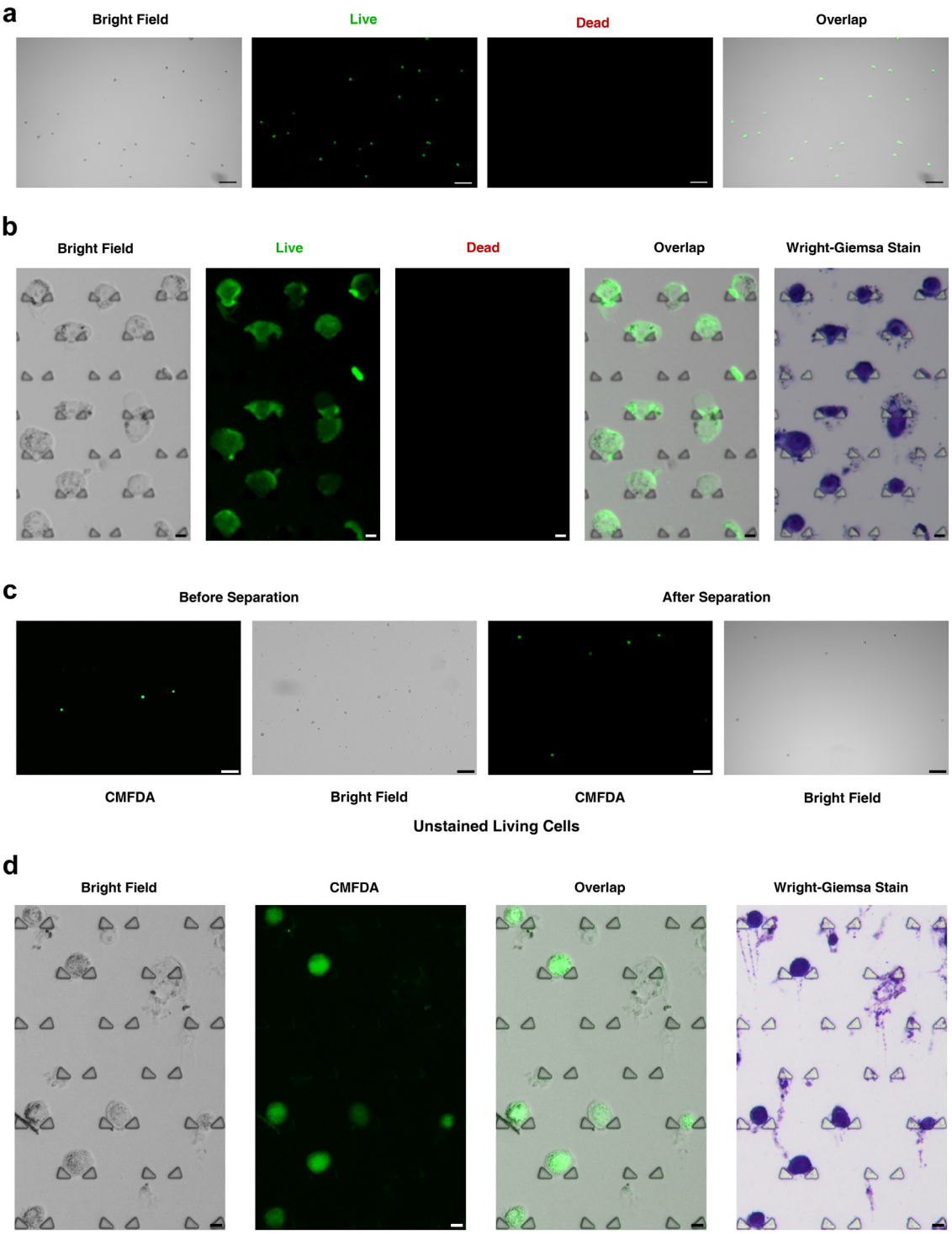

***Fig. 7*: The ability of our devices to separate and analyze living cells.** (a) Live-Dead Cell Staining on collected cells in the cancer outlet of the IMD, Scale bar, 100 μm. (b) Live-Dead Cell Staining and Wright-Giemsa staining on cells in the SCTA-chip, Scale bar, 8 μm (The minimum gap of a single cell trap, 8 μm). (c) Fluorescence images of samples of unstained living cells before and after IMD separation. We mixed HGC-27 cells, which were incubated with CellTracker Green CMFDA, with fresh peritoneal lavage cells at a 1:10 ratio, Scale bar, 100 μm. (d) Wright-Giemsa staining on separated living cancer cells in the SCTA-chip, Scale bar, 8 μm (The minimum gap of a single cell trap, 8 μm).

integrated microfluidic chip. However, in actuality, the calculated Dc values are all approximate. Apart from different theories for calculation, Dc may also be influenced by multiple factors including roughness inside the chip, and sample density and viscosity. Therefore, the separation efficiency of devices should be examined by practical experiments. Subsequently, cancer cells were injected into the integrated microfluidic chip to measure recovery rate. The recovery rates above 80% reflected the ability of our device to collect the majority of the cancer cells in the sample. However, some cells with larger diameter showed relative lower recovery rates, such as SNU-5 compared to SNU-16 at 50 and 500 cells, and MKN-28 compared to AGS at 500 cells. Cell separation on our device mainly depends on cell size, but separation efficiency may not be strictly proportionate to cell size. Beech reported that biological particles can interact with the posts in the DLD and cause flow perturbation.[41] Cells with sizes similar to the gap distance (30 μm in our manuscript) are more apt to cause flow perturbation. The diameters of the seven cancer cell lines used in our manuscript ranged from 15.98 μm to 21.74 μm, thus flow perturbation may be more likely to influence recovery of the larger cells. Furthermore, cells with different nucleocytoplasmic ratios likely also have different cell density. Due to the combined effects of gravity, buoyancy, and fluid resistance, cells with different densities may have different sedimentation velocities, resulting in different focusing positions in the spiral channel. These factors may influence sorting effect. Beech also demonstrated that cell deformability and shape may further influence their trajectory in DLD devices.[41,47]

We then mixed a GC cell line with hysteromyoma lavage cells in different proportions to simulate ascites and peritoneal lavages. The ratio of 1:10 is similar to that of cancer cells and background cells in ascites; ratios of 1:100, 1:1000 and 1: 10,000 are similar to that of cancer cells and background cells in peritoneal lavages of patients with GC.[48] The results proved that our device could separate cancer cells even from simulated samples at a ratio of 1:10,000. Moreover, our integrated microfluidic chip could achieve high-throughput separation with a speed of 100 μL/min, which solves the disadvantage of blockage seen when running at high velocity using a single DLD chip. This enables samples with large numbers of cells to be screened and isolated, laying a solid foundation for the application of this device in separating cells from pure clinical specimens in the future.

We next collected ascites samples from 12 patients with GC and separated cancer cells from the ascites. Studies performing cell separation from patients' ascites based on physical methods are rare, and our study realized cancer cells separation from complete patients' ascites using an integrated microfluidic chip. To verify the concentrating effect of our device, the separated cells were stained using the ThinPrep Papanicolaou method, then compared with the results before cell separation. The device successfully increased the number of cancer cells in the field of vision and reduced background cells. This will greatly facilitate the identification of tumor cells in clinical ascites samples and help diagnose early peritoneal metastasis by overcoming the difficulty of finding tumor cells within a large amount of background cells. Our device could improve the sensitivity of traditional detection methods. Furthermore, the separation process was relatively short, making it convenient to operate in clinic and indicating that our integrated microfluidic chip may impact clinical practice by serving as an auxiliary method for clinical cytological tests.

In our study, we achieved unbiased cell separation without losing cells with different phenotypes based on physical cellular characteristics. On this basis, we used the SCTA-chip to analyze separated cells at the single cell level. The SCTA-chip provides a relatively fixed position for cancer cells, allowing us to perform more than one analysis method on the collected cells. As such, we could analyze and compare multiple characteristics and gather additional information for each individual cell. Moreover, SCTA-chips avoid cell loss during cell staining (especially during flushing) by capturing the cancer cells in traps. In the SCTA-chip, the accuracy and purity of the separation was further verified with Wright-Giemsa staining. At the same time, we also tested EpCAM, Yap1, and CD45 expression in separated cells by immunofluorescence to provide more evidence. EpCAM is a diagnostic biomarker of epithelial malignancies.[28,42,43] Ajani et al. reported YAP1 as a specific marker of tumor cells in ascites, with high expression in the tumor cells of peritoneal metastasis regardless of EpCAM expression.[15] CD45 is a classical immune cell marker widely expressed in all leukocytes. We selected these three biomarkers to verify whether the separated cells were cancer cells. Immunofluorescence results showed that the cells separated from 12 ascites samples were all EpCAM-positive and CD45-negative. Furthermore, separated cells from ten of the 12 samples were positive for both EpCAM and YAP1, proving that the separated cells were cancer cells. We concurrently performed Wright-Giemsa staining on the separated cells in the SCTA-chip. We chose Wright-Giemsa staining rather than Papanicolaou staining, which is more common in clinics, because Wright-Giemsa staining is simpler to operate and able to distinguish GC cells. The collected cells were mostly hyperchromatic and had large nuclei, further proving that the separated cells were cancer cells. Based on this, we calculated the overall purity of the separation to be 73% via pooled analysis on Stata software. The separated cells did include some noncancer cells. This may be due to the reason that some noncancer cells were larger than 10 μm in diameter. Nevertheless, the purity of 73% was higher than previous finding[48] and achieve the best

performance in ascites cancer cell separation. Given that our method could achieve high throughout and high purity cell separation, combining our microfluidic devices with pathological examinations may have a good prospect in improving peritoneal metastasis diagnosis.

Besides separation, characterizing cancer cells is also important. Moreover, SCTA-chips avoid cell loss during cell staining (especially during flushing) by capturing the cancer cells in traps. Therefore, we chose SCTA-chip for cell analysis. We collected primary cancer lesions from six patients, as well as NATs and metastasis lymph node/TD from four patients (P04, P05, P06, and P07). In our study, metastatic lymph nodes and TD represented metastatic tissues for GC. As early as 1935, Gabriel et al. proposed the concept of TD.[49] TD is defined as focal aggregates of adenocarcinoma in the fat around the tumor which are discontinuous with primary tumors and independent of the lymph nodes.[50] Similar to lymph node metastasis, TD can be considered a form of metastasis.[51,52] Through IHC, we explored gene expression patterns in primary lesions, NAT, metastatic lymph nodes/TD, and ascites cancer cells.

We also explored the expression pattern of YAP1 in ascites cancer cells and tissues. In our study, YAP1 is not only a marker to distinguish cancer cells, but also a useful marker for serial gene analysis. YAP1 has been reported to play an oncogenic role in cancer progression and metastases.[53] It is suggested that YAP1 could be pursued as a promising therapeutic target against GC peritoneal metastasis. They showed that YAP1 plays an essential role in peritoneal carcinomatosis and that peritoneal carcinomatosis could be attenuated by YAP1 inhibition.[15] In our study, four of the collected samples included primary lesions and NAT. In half of the samples, YAP1 expression was higher in the primary lesions than in NAT. YAP1 had similar high expression in the primary lesion and NAT in another sample. This is consistent with previous studies and reflects that YAP1 overexpression is a sign of cancer.[13] We then explored the changes in YAP1 expression across different cancerous tissues and cells. When comparing primary lesions with ascites cancer cells, YAP1 expression was similar in four out of six samples, with high YAP1 expression (IHC score $\geq$2) in the primary lesions and positive expression in ascites cancer cells. Another two samples showed different expression patterns, with one (P09) having high YAP1 expression in the primary lesion but negative in ascites cancer cells and the other (P05) having low YAP1 expression in the primary lesion with positive expression in ascites cells. Interestingly, the primary and metastatic tissue for P05 also showed different expression patterns, with low YAP1 in the primary lesion and high expression in metastatic lymph nodes. The YAP1 expression in metastatic cells (ascites cancer cells, metastatic lymph nodes, or TD) was in accordance across sites. Our findings demonstrate that YAP1 expression in tumor cells may change during the metastasis process. Similarly, Lee et al. reported that YAP1 is essential for lymph node metastasis and that it becomes more expressed in metastatic tumors.[14] Altogether, our data suggests the necessity of exploring YAP1 expression in ascites cancer cells to facilitate targeted therapy, and our study provides a method for achieving this target.

Trastuzumab, the most important drug in targeted therapy, has shown benefits for overall survival when added to chemotherapy for HER-2-positive advanced GC.[17] It is reported that the HER-2 positive rate ranges from 9 to 28% in primary GC tissues.[9,54,55] Although targeted therapy is applied to control metastasis, molecular status is usually evaluated in the primary lesions since metastatic lesions are difficult to biopsy, especially for peritoneal metastasis.[56] Through SCTA chip, we detected HER-2 expression in ascites cancer cells at the single cell level. The results showed that ascites cancer cells from 8 out of 12 samples showed HER-2 positivity, well higher than the HER-2 positivity detected in primary GC tissues by previous studies.[54,55] Discordant HER-2 status between primary and metastatic GC is not rare.[9,10] Peng et al. showed a positive conversion rate of HER-2 (negative in primary lesions but positive in metastatic lesions) of 4% for GC in a meta-analysis of 13 studies.[9] The conversion rate was 9.5% in breast cancer, as shown by Schrijver et al. through meta-analysis.[57] Our study also compared HER-2 expression between primary and metastatic GC tissues or cells. Two out of six patients showed discordant HER-2 status between their primary lesions and ascites cancer cells, with HER-2 negative or low expressed in primary lesions but positive in ascites cancer cells. Though this discordance may explain the phenomenon of higher HER-2 expression in ascites cancer cells, 8 out of 12 samples of ascites cancer cells presenting as HER-2^{+} appeared unexpectedly high, considering how the other metastatic tissues (e.g. LN metastasis, liver metastasis) showed similar overall HER-2 positivity as the primary GC tissues.[9,10,56] We suggest that more ascites GC cells and paired primary cancer tissues should be tested at the single cell level to expand upon our results and provide more solid evidence in the future. Nevertheless, our data demonstrates that HER-2 may be highly expressed in ascites cancer cells, suggesting that targeted therapy by trastuzumab could be a future therapeutic and investigation direction for GC peritoneal metastasis.

Ascites samples in our paper were from a biobank collection stored at –80 °C, and freeze-thawed unfixed cells were seen to break into fragments during the separation and analysis processes in the microfluidic chips. This may result from cells in microchips being affected by shear stress, especially in SCTA chips[58] and under high flow rate in DLD chips.[59] Thus, we fixed our cells with paraformaldehyde to enhance our success rate in cell sorting and trapping for samples from the biobank. Paraformaldehyde fixation can increase tissue

stiffness[60] and preserve call shape[61,62] by inducing covalent cross-linking between molecules, effectively gluing them together into an insoluble meshwork.[63] After paraformaldehyde, almost no cells showed cell lysis in our chips. Then, we further tested the ability of our devices for separating and analyzing living cells. We injected HGC-27 cells into the IMD and SCTA-chip, and live-dead cell staining results proved that our device could be used for living cells. We then mixed living HGC-27 GC cells with fresh peritoneal lavage cells at a 1:10 proportion and performed separation by IMD, obtaining recovery and purity comparable to those with fixed cells. Nevertheless, the efficiency of our devices in separating fresh ascites samples should be expanded upon in future studies. Moreover, we suggest that if our devices are utilized clinically, then fresh samples should be examined as soon as possible if they are not fixed for analysis.

The size difference between tumor cells and background cells provides the theoretical basis for most microfluidic techniques that separate tumor cells.[36] Examples of this are seen in Warkiani et al. isolating spiked cell lines from lysed blood samples[35]; Chiu et al. separating PC-3 cancer cells from leukocytes[64]; and Wu et al. sorting prostate cancer cells from whole blood samples.[23] In our study, we designed an integrated microfluidic chip combining DFF and DLD, utilizing the unique characteristics of both chips to achieve high-throughput separation of GC cells from ascites. Our study realized cancer cells separation from complete patients' ascites through an integrated microfluidic chip. We also compared the efficiency of the IMD with individual chips. The results showed that the IMD had better efficiency (section 3.3), proving the benefit of combining the chips. However, the flow rate used in our manuscript (at which the IMD has the best separation efficiency) may not be the most ideal flow rate for each individual device. The flow resistance of the individual DFF chip is different from that experienced in the integrated microfluidic device (IMD) at the same flow rate.[65] Cells are subjected to different forces in a DFF on an IMD compared to in an individual DFF chip, leading to different focusing positions of cells between the IMD and the individual DFF chip. Therefore, the separation efficiency of the spiral chip in the IMD and the individual DFF is different under the same flow rate, and the recovery rate of the DFF alone is relatively lower when run at the ideal flow rate for the IMD. For the cell density used in our study, the individual DLD chip has high recovery rates for cell separation at a relative low flow rate, but cells will clog when the flow rate increases. However, in the IMD, the DFF spiral chip performs an initial cell separation and enrichment process, greatly improving the concentration and purity of the cancer cells entering the DLD chip. This causes cells to avoiding clogging once they are in the DLD even at a high flow rate. Thus, under the flow rate used for the IMD, cells will clog if the DLD chip is run individually, leading to low recovery rate. To expand on this idea, we compared our IMD results with previous studies that separated cells using individual DFF[27,66–68] or DLD[27,34,37,69] techniques (Supplementary Table S2). Compared with individual DFF and DLD chips operating at their ideal flow rates, the IMD still simultaneously showed higher recovery rate, purity, and throughput. Moreover, the mix ratio of our study (down to 1:10,000) was also lower than in most studies. These findings support the superiority and necessity of integrating the DFF and DLD techniques.

There are some limitations to our study. First, we fixed and filtered the clinical ascites cells before separation. These processes cause a certain amount of cell loss. To test cell loss, we counted 8.0×10^5 ascites cells before cell preparation and found that 74.7% ± 4.30% (average 6.0×10^5 cells) remained after filtration and fixation. Therefore, for clinical samples undergoing filtration and fixation, the proportion of recovered cancer cells compared to initial cell count may be lower than the IMD recovery rate reported in the manuscript. We demonstrated that the proportion of recovered cancer cells compared to initial cell count is around 63%, since 74.7% of cells remained after filtration and fixation and then the recovery rate of the IMD device is around 85%. This decreased recovery rate for clinical samples may limit the clinical utilization of our method. We suggest that if our devices are utilized clinically in the future, it would be optimal to use fresh samples and separate cancer cells as soon as possible to avoid cell lysis. Secondly, cancer cells less than Dc were not separated in our study. Also, since radical surgery is not recommended for GC patients with peritoneal metastasis, we collected only 6 primary lesions and 4 metastatic tissues samples. Future serial molecular expression analysis is needed from more samples to expand our results. We also tried to provide a more automated system by integrating the SCTA chip into the IMD. However, the most important reason that we did not perform this integration was that these two chips have distinctly different flow rates. The flow rate of the IMD was 100 μL/min, while the flow rate of the SCTA-chip was 12 μL/min. Another reason was that cells in the SCTA-chip need to undergo complex staining procedures which were unnecessary for cells in the IMD.

In summary, we achieved rapid and label-free separation of tumor cells from ascites and peritoneal lavages using an IMD based on hydrodynamics. Our device could concentrate GC cells with high throughput, making it easier for pathologists to find cancer cells in ascites and showing its potential to impact clinical practice and serving as an auxiliary method for clinical cytological testing. Furthermore, we analyzed the separated cells at the single-cell level using an SCTA-chip. The separated cells were identified as cancer cells

based on immunofluorescence imaging and Wright-Giemsa staining. The overall purity of separation was analyzed with Wright-Giemsa staining and calculated to be 73%. We found an unexpectedly high HER-2 positivity rate in ascites cancer cells, highlighting the need for further verification in larger samples. Our study could provide a method to investigate therapeutic targets and strategies for GC peritoneal metastasis.

Contributors

Junhua Zhao: Investigation, visualization, writing-original draft. Zhaojun Han: Investigation, visualization, writing-original draft. Chang Xu: Resources, writing-original draft. Lu Li: Conceptualization, writing-review & editing. Haimeng Pei: Visualization, writing-original draft. Yongxi Song: Conceptualization, investigation, resources, writing-review & editing. Zhenning Wang: Conceptualization, investigation, resources, writing-review & editing. Bo Tang: Conceptualization, investigation, resources, writing-review & editing. Junhua Zhao, Zhaojun Han, Chang Xu, Yongxi Song, Zhenning Wang and Bo Tang have verified the underlying data. All authors have read and approved the final version of the manuscript.

Data sharing statement

All data needed to evaluate the conclusions in the paper are present in the paper and/or the Supplementary Materials.

Declaration of interests

The authors declare no conflict of interest.

Acknowledgments

We thank Professor Xiaoyi Mi from Pathology Department of First Hospital of China Medical University and Doctor Xin Wei from Hematology Department of First Hospital of China Medical University for their help in pathological diagnosis. We thank Professor Cheng Chen from Hefei PreceDo pharmaceuticals Co. Ltd. for his technical assistance in the preservation and transportation of fresh peritoneal lavages. We thank Doctor Di Zhu from Pathology Department of First Hospital of China Medical University for her technical assistance in ThinPrep Papanicolaou staining. This research was supported by National Natural Science Foundation of China, China (22134004, U1908207, 91859111); Natural Science Foundation of Shandong Province of China, China (ZR2019JQ06); Taishan Scholars Program of Shandong Province tsqn, China (201909077); Local Science and Technology Development Fund Guided by the Central Government, China (YDZX20203700002568). Applied Basic Research Program of Liaoning Province, China (2022020284-JH2/1013).

Appendix A. Supplementary data

Supplementary data related to this article can be found at https://doi.org/10.1016/j.ebiom.2023.104522.

References

1 Joshi SS, Badgwell BD. Current treatment and recent progress in gastric cancer. *CA Cancer J Clin*. 2021;71(3):264–279.
2 Salati M, Orsi G, Smyth E, et al. Gastric cancer: translating novels concepts into clinical practice. *Cancer Treat Rev*. 2019;79:101889.
3 Higaki E, Yanagi S, Gotohda N, et al. Intraoperative peritoneal lavage cytology offers prognostic significance for gastric cancer patients with curative resection. *Cancer Sci*. 2017;108(5):978–986.
4 Kanda M, Kodera Y. Molecular mechanisms of peritoneal dissemination in gastric cancer. *World J Gastroenterol*. 2016;22(30):6829–6840.
5 Dong D, Tang L, Li ZY, et al. Development and validation of an individualized nomogram to identify occult peritoneal metastasis in patients with advanced gastric cancer. *Ann Oncol*. 2019;30(3):431–438.
6 Wong J, Coit D. Detection of gastric cancer peritoneal metastases by peritoneal lavage: current limitations and future perspectives. *Surgery*. 2012;152(1):1–4.
7 Taffon C, Giovannoni I, Mozetic P, et al. Seriate cytology vs molecular analysis of peritoneal washing to improve gastric cancer cells detection. *Diagn Cytopathol*. 2019;47(7):670–674.
8 Yáñez-Mó M, Lara-Pezzi E, Selgas R, et al. Peritoneal dialysis and epithelial-to-mesenchymal transition of mesothelial cells. *N Engl J Med*. 2003;348(5):403–413.
9 Peng Z, Zou J, Zhang X, et al. HER2 discordance between paired primary gastric cancer and metastasis: a meta-analysis. *Chin J Cancer Res*. 2015;27(2):163–171.
10 Fusco N, Rocco EG, Del Conte C, et al. HER2 in gastric cancer: a digital image analysis in pre-neoplastic, primary and metastatic lesions. *Mod Pathol*. 2013;26(6):816–824.
11 Tumaneng K, Russell RC, Guan KL. Organ size control by Hippo and TOR pathways. *Curr Biol*. 2012;22(9):R368–R379.
12 Tumaneng K, Schlegelmilch K, Russell RC, et al. YAP mediates crosstalk between the Hippo and PI(3)K–TOR pathways by suppressing PTEN via miR-29. *Nat Cell Biol*. 2012;14(12):1322–1329.
13 Zanconato F, Cordenonsi M, Piccolo S. YAP/TAZ at the roots of cancer. *Cancer Cell*. 2016;29(6):783–803.
14 Lee CK, Jeong SH, Jang C, et al. Tumor metastasis to lymph nodes requires YAP-dependent metabolic adaptation. *Science*. 2019;363(6427):644–649.
15 Ajani JA, Xu Y, Huo L, et al. YAP1 mediates gastric adenocarcinoma peritoneal metastases that are attenuated by YAP1 inhibition. *Gut*. 2021;70(1):55–66.
16 Gravalos C, Jimeno A. HER2 in gastric cancer: a new prognostic factor and a novel therapeutic target. *Ann Oncol*. 2008;19(9):1523–1529.
17 Bang YJ, Van Cutsem E, Feyereislova A, et al. Trastuzumab in combination with chemotherapy versus chemotherapy alone for treatment of HER2-positive advanced gastric or gastro-oesophageal junction cancer (ToGA): a phase 3, open-label, randomised controlled trial. *Lancet*. 2010;376(9742):687–697.
18 Gao R, Zhan C, Wu C, et al. Simultaneous single-cell phenotype analysis of hepatocellular carcinoma CTCs using a SERS-aptamer based microfluidic chip. *Lab Chip*. 2021;21(20):3888–3898.
19 You SM, Luo K, Jung JY, et al. Gold nanoparticle-coated starch magnetic beads for the separation, concentration, and SERS-based detection of E. coli O157:H7. *ACS Appl Mater Interfaces*. 2020;12(16):18292–18300.
20 Yoshioka J, Ohsugi Y, Yoshitomi T, Yasukawa T, Sasaki N, Yoshimoto K. Label-free rapid separation and enrichment of bone marrow-derived mesenchymal stem cells from a heterogeneous cell mixture using a dielectrophoresis device. *Sensors (Basel)*. 2018;18(9):3007.
21 Kung YC, Niazi KR, Chiou PY. Tunnel dielectrophoresis for ultra-high precision size-based cell separation. *Lab Chip*. 2021;21(6):1049–1060.
22 Wang K, Zhou W, Lin Z, et al. Sorting of tumour cells in a microfluidic device by multi-stage surface acoustic waves. *Sens Actuators B Chem*. 2017;258.
23 Wu M, Huang PH, Zhang R, et al. Circulating tumor cell phenotyping via high-throughput acoustic separation. *Small*. 2018;14(32):e1801131.
24 Arai F, Ng C, Maruyama H, Ichikawa A, El-Shimy H, Fukuda T. On chip single-cell separation and immobilization using optical tweezers and thermosensitive hydrogel. *Lab Chip*. 2005;5(12):1399–1403.
25 Liu S, Li Z, Weng Z, et al. Miniaturized optical fiber tweezers for cell separation by optical force. *Opt Lett*. 2019;44(7):1868–1871.
26 Lin E, Rivera-Báez L, Fouladdel S, et al. High-throughput microfluidic labyrinth for the label-free isolation of circulating tumor cells. *Cell Syst*. 2017;5(3):295–304.e4.
27 Zeming KK, Sato Y, Yin L, et al. Microfluidic label-free bioprocessing of human reticulocytes from erythroid culture. *Lab Chip*. 2020;20(18):3445–3460.
28 Bhagat AA, Kuntaegowdanahalli SS, Papautsky I. Continuous particle separation in spiral microchannels using Dean flows and differential migration. *Lab Chip*. 2008;8(11):1906–1914.
29 Huang LR, Cox EC, Austin RH, Sturm JC. Continuous particle separation through deterministic lateral displacement. *Science*. 2004;304(5673):987–990.
30 McGrath J, Jimenez M, Bridle H. Deterministic lateral displacement for particle separation: a review. *Lab Chip*. 2014;14(21):4139–4158.
31 Loutherback K, D'Silva J, Liu L, Wu A, Austin RH, Sturm JC. Deterministic separation of cancer cells from blood at 10 mL/min. *AIP Adv*. 2012;2(4):42107.

32 Wang J, Lu W, Tang C, et al. Label-free isolation and mRNA detection of circulating tumor cells from patients with metastatic lung cancer for disease diagnosis and monitoring therapeutic efficacy. *Anal Chem*. 2015;87(23):11893–11900.
33 Edd JF, Mishra A, Dubash TD, et al. Microfluidic concentration and separation of circulating tumor cell clusters from large blood volumes. *Lab Chip*. 2020;20(3):558–567.
34 Tran TSH, Ho BD, Beech JP, Tegenfeldt JO. Open channel deterministic lateral displacement for particle and cell sorting. *Lab Chip*. 2017;17(21):3592–3600.
35 Warkiani ME, Khoo BL, Wu L, et al. Ultra-fast, label-free isolation of circulating tumor cells from blood using spiral microfluidics. *Nat Protoc*. 2016;11(1):134–148.
36 Xu X, Jiang Z, Wang J, Ren Y, Wu A. Microfluidic applications on circulating tumor cell isolation and biomimicking of cancer metastasis. *Electrophoresis*. 2020;41(10–11):933–951.
37 Okano H, Konishi T, Suzuki T, et al. Enrichment of circulating tumor cells in tumor-bearing mouse blood by a deterministic lateral displacement microfluidic device. *Biomed Microdevices*. 2015;17(3):9964.
38 Zhang Z, Henry E, Gompper G, Fedosov DA. Behavior of rigid and deformable particles in deterministic lateral displacement devices with different post shapes. *J Chem Phys*. 2015;143(24):243145.
39 Cho EY, Park K, Do I, et al. Heterogeneity of ERBB2 in gastric carcinomas: a study of tissue microarray and matched primary and metastatic carcinomas. *Mod Pathol*. 2013;26(5):677–684.
40 Inglis DW, Davis JA, Austin RH, Sturm JC. Critical particle size for fractionation by deterministic lateral displacement. *Lab Chip*. 2006;6(5):655–658.
41 Beech J. *Microfluidics separation and analysis of biological particles*. Lund, Sweden: Lund University; 2011.
42 Eslami SZ, Cortés-Hernández LE, Alix-Panabières C. Epithelial cell adhesion molecule: an anchor to isolate clinically relevant circulating tumor cells. *Cells*. 2020;9(8):1836.
43 Gires O, Pan M, Schinke H, Canis M, Baeuerle PA. Expression and function of epithelial cell adhesion molecule EpCAM: where are we after 40 years? *Cancer Metastasis Rev*. 2020;39(3):969–987.
44 Dahlke MH, Larsen SR, Rasko JE, Schlitt HJ. The biology of CD45 and its use as a therapeutic target. *Leuk Lymphoma*. 2004;45(2):229–236.
45 Rheinländer A, Schraven B, Bommhardt U. CD45 in human physiology and clinical medicine. *Immunol Lett*. 2018;196:22–32.
46 Alroy I, Yarden Y. The ErbB signaling network in embryogenesis and oncogenesis: signal diversification through combinatorial ligand-receptor interactions. *FEBS Lett*. 1997;410(1):83–86.
47 Beech JP, Holm SH, Adolfsson K, Tegenfeldt JO. Sorting cells by size, shape and deformability. *Lab Chip*. 2012;12(6):1048–1051.
48 Zhang Y, Zhao J, Yu H, et al. Detection and isolation of free cancer cells from ascites and peritoneal lavages using optically induced electrokinetics (OEK). *Sci Adv*. 2020;6(32):eaba9628.
49 Gabriel WBDC, Bussey HJR. Lymphatic spread in cancer of the rectum. *Br J Surg*. 1935;23.
50 Ueno H, Mochizuki H, Shirouzu K, et al. Multicenter study for optimal categorization of extramural tumor deposits for colorectal cancer staging. *Ann Surg*. 2012;255(4):739–746.
51 Etoh T, Sasako M, Ishikawa K, Katai H, Sano T, Shimoda T. Extranodal metastasis is an indicator of poor prognosis in patients with gastric carcinoma. *Br J Surg*. 2006;93(3):369–373.
52 Lee HS, Lee HE, Yang HK, Kim WH. Perigastric tumor deposits in primary gastric cancer: implications for patient prognosis and staging. *Ann Surg Oncol*. 2013;20(5):1604–1613.
53 Kang W, Tong JH, Chan AW, et al. Yes-associated protein 1 exhibits oncogenic property in gastric cancer and its nuclear accumulation associates with poor prognosis. *Clin Cancer Res*. 2011;17(8):2130–2139.
54 Yu GZ, Chen Y, Wang JJ. Overexpression of Grb2/HER2 signaling in Chinese gastric cancer: their relationship with clinicopathological parameters and prognostic significance. *J Cancer Res Clin Oncol*. 2009;135(10):1331–1339.
55 Barros-Silva JD, Leitão D, Afonso L, et al. Association of ERBB2 gene status with histopathological parameters and disease-specific survival in gastric carcinoma patients. *Br J Cancer*. 2009;100(3):487–493.
56 Shinozaki E, Yamamoto N, Saiura A, et al. Concordance of HER2 and its related molecules between primary and paired liver metastatic sites in gastric cancer. *J Clin Oncol*. 2013;31(15_suppl):4108.
57 Schrijver W, Suijkerbuijk KPM, van Gils CH, van der Wall E, Moelans CB, van Diest PJ. Receptor conversion in distant breast cancer metastases: a systematic review and meta-analysis. *J Natl Cancer Inst*. 2018;110(6):568–580.
58 Kobel S, Valero A, Latt J, Renaud P, Lutolf M. Optimization of microfluidic single cell trapping for long-term on-chip culture. *Lab Chip*. 2010;10(7):857–863.
59 Hochstetter A, Vernekar R, Austin RH, et al. Deterministic lateral displacement: challenges and perspectives. *ACS Nano*. 2020;14(9):10784–10795.
60 Iwashita M, Nomura T, Suetsugu T, Matsuzaki F, Kojima S, Kosodo Y. Comparative analysis of brain stiffness among amniotes using glyoxal fixation and atomic force microscopy. *Front Cell Dev Biol*. 2020;8:574619.
61 Li Y, Almassalha LM, Chandler JE, et al. The effects of chemical fixation on the cellular nanostructure. *Exp Cell Res*. 2017;358(2):253–259.
62 Baczewska M, Eder K, Ketelhut S, Kemper B, Kujawinska M. Refractive index changes of cells and cellular compartments upon paraformaldehyde fixation acquired by tomographic phase microscopy. *Cytometry A*. 2021;99(4):388–398.
63 Thavarajah R, Mudimbaimannar VK, Elizabeth J, Rao UK, Ranganathan K. Chemical and physical basics of routine formaldehyde fixation. *J Oral Maxillofac Pathol*. 2012;16(3):400–405.
64 Chiu TK, Chou WP, Huang SB, et al. Application of optically-induced-dielectrophoresis in microfluidic system for purification of circulating tumour cells for gene expression analysis- Cancer cell line model. *Sci Rep*. 2016;6:32851.
65 Abdulla A, Liu W, Gholamipour-Shirazi A, Sun J, Ding X. High-throughput isolation of circulating tumor cells using cascaded inertial focusing microfluidic channel. *Anal Chem*. 2018;90(7):4397–4405.
66 Nagrath S, Sequist LV, Maheswaran S, et al. Isolation of rare circulating tumour cells in cancer patients by microchip technology. *Nature*. 2007;450(7173):1235–1239.
67 Zhu Z, Li S, Wu D, et al. High-throughput and label-free enrichment of malignant tumor cells and clusters from pleural and peritoneal effusions using inertial microfluidics. *Lab Chip*. 2022;22(11):2097–2106.
68 Hou HW, Warkiani ME, Khoo BL, et al. Isolation and retrieval of circulating tumor cells using centrifugal forces. *Sci Rep*. 2013;3:1259.
69 Siyang Z, Yung R, Yu-Chong T, Kasdan H, eds. *Deterministic lateral displacement MEMS device for continuous blood cell separation. 18th IEEE international conference on micro electro mechanical systems, 2005 MEMS 2005; 2005 30 Jan.-3 Feb*. 2005.